Kinetic analysis makes the impossible possible: measuring CO adsorption free energies on the active sites during CO_2 electroreduction

Zhihao Cui[1*], Kassidy D. Aztergo[1], Jiseon Hwang[1], and Anne C. Co[1*]

[1]Department of Chemistry and Biochemistry, The Ohio State University, Columbus, Ohio, 43210, USA

[*]Corresponding author: Anne C. Co (co.5@osu.edu); Zhihao Cui (cui.591@osu.edu)

TOC figure

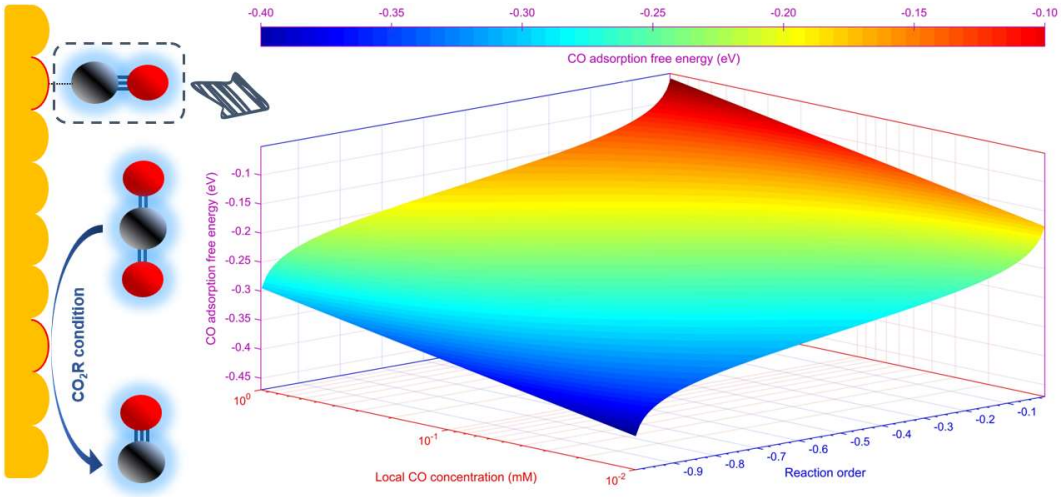

Abstract

CO adsorption free energy (ΔG_{CO}^{ads}) was proposed as an important descriptor for CO_2 electroreduction (CO_2R), but this hypothesis has not been verified due to the lack of an experimental method that can measure ΔG_{CO}^{ads} during CO_2R. Herein, we develop a universal kinetic model combined with a rotating ring-disk electrode voltammetry method to estimate ΔG_{CO}^{ads} on the active sites of various CO-producing catalysts during CO_2R. We find CO adsorption is affected by the catalyst, cation identity, cation concentration, applied potential, and surface structure at CO_2R condition. We also find that ΔG_{CO}^{ads} difference is insignificant between Au and Cu, which cannot account for the observation that only Cu can catalyze CO_2 to multicarbon products with substantial rates. This work highlights the complexity of evaluating CO adsorption at CO_2R condition and provides an experimental approach based on kinetic analysis for measuring ΔG_{CO}^{ads} on the active sites of CO-producing catalysts during CO_2R.

Introduction

CO_2 electroreduction (CO_2R) driven by renewable electricity provides an attractive route to produce sustainable fuels and chemicals [1,2]. Although CO_2 can be converted to CO on various catalysts through a two-electron transfer process, the further reduction of CO to more valuable products, such as multicarbon hydrocarbons and oxygenates, was only observed on a limited number of catalysts [3,4], mainly Cu-based catalysts. Despite intense efforts to search for a more efficient electrocatalyst than Cu [5-9], the search remains fruitless due to the lack of a rational design principle for catalysts that can electrochemically reduce CO_2 to multicarbon products.

To understand the origin of the product selectivity on various CO_2R catalysts, a prevalent hypothesis is that CO adsorption energy is a key descriptor to determine the product selectivity trend across different catalysts for CO_2R [10]. For example, Au and Ag catalysts display extremely high selectivity toward CO due to their relatively weak CO binding strengths which facilitate CO desorption, whereas Cu can further reduce the adsorbed CO to multicarbon products due to its intermediate CO binding strength. However, these correlations were obtained from comparing experimentally measured

CO_2R selectivity with DFT-calculated CO binding energies under vacuum condition. Since CO adsorption happens at a more complex electrode-electrolyte interface rather than a simple solid-vacuum interface during CO_2R, CO adsorption is expected to be influenced by both the electrical double layer (EDL) structure [11] and the electrode potential [12-14]. Therefore, the reliability of using DFT-calculated CO adsorption energy as a descriptor needs to be verified by measuring CO adsorption free energies at CO_2R conditions through an experimental approach.

Even though CO adsorption has been extensively investigated with various techniques under ultrahigh vacuum conditions [15-17], to the best of our knowledge, there is no experimental approach available to measure CO adsorption free energies on surface active sites under CO_2R conditions. Recently, Xu group developed a novel surface enhanced infrared absorption spectroscopy (SEIRAS) method to estimate the adsorption enthalpy of CO from the Van 't Hoff equation on the dendritic Cu electrode [18]. They showed that measured CO adsorption enthalpy alone cannot be used as a universal descriptor for the observed selectivity trend toward multicarbon products across various Cu-based catalysts during CO_2R [19], highlighting the knowledge gap between the actual CO_2R condition and DFT modeling in vacuum. Note that CO adsorption enthalpy is not a complete thermodynamic descriptor because adsorption entropy may also play an important role in CO adsorption process. It is likely that CO adsorption enthalpy fails to predict the selectivity trend because the adsorption entropy effect is not properly included in the descriptor. To address the aforementioned knowledge gap and determine whether CO adsorption free energy is an effective descriptor, there is an urgent need to develop an experimental method to estimate CO adsorption free energies (ΔG_{CO}^{ads}) on surface active sites at CO_2R condition.

In this work, a universal kinetic model combined with a rotating ring-disk electrode (RRDE) voltammetry method was developed to measure ΔG_{CO}^{ads} on the active sites of CO-producing catalysts during CO_2R. Specifically, we first measured local CO concentrations and CO reaction orders during CO_2R using a RRDE voltammetry method on Au, Cu, glassy carbon supported cobalt phthalocyanine, Au(110), and Au(111) electrodes in different electrolytes, then the obtained data was plugged into the kinetic expression to derive ΔG_{CO}^{ads}. Based on measured data, we observed that there are at least five factors affecting CO adsorption under CO_2R conditions: catalyst identity,

cation identity, cation concentration, applied potential and surface structure. We found a small difference of ΔG_{CO}^{ads} between Au and Cu at CO_2R condition. Therefore, we conclude ΔG_{CO}^{ads} alone is unlikely an efficient descriptor for the formation of multicarbon products during CO_2R. The unique experimental method presented in this work provides a crucial foundation for understanding and theoretical modeling of complex electrochemical CO and CO_2 reduction.

Results

Derivation of a universal kinetic expression for estimating ΔG_{CO}^{ads} on surface active sites of CO-producing catalysts during CO_2R

To estimate the ΔG_{CO}^{ads} on various CO-producing catalysts during CO_2R, a kinetic model is proposed through considering the first electron transfer step as the rate-limiting step (RLS), which is commonly accepted as the RLS of CO_2R to CO on various heterogeneous electrocatalysts such as polycrystalline Au, Ag, Cu and glassy carbon supported cobalt phthalocyanine (CoPc/GC) [20-23], although whether a proton transfer is involved in the RLS is still a topic under debate [24-26]. Nevertheless, we will show that the derived kinetic expression for estimating ΔG_{CO}^{ads} remains the same for a RLS with or without a proton transfer in a mean-field kinetic model. First, we consider the following reaction steps when the RLS is a CO_2 adsorption with an electron transfer step during CO_2R in neutral media:

$$CO_2 + e^- + * \xrightarrow{\overrightarrow{k_{1a}}} CO_2^{-*} \quad (1a)$$

$$CO_2^{-*} + H_2O + e^- \xrightarrow{\overrightarrow{k_{2a}}} CO^* + 2OH^- \quad (2a)$$

$$CO^* \underset{\overleftarrow{k_3}}{\overset{\overrightarrow{k_3}}{\rightleftharpoons}} CO + * \quad (3)$$

Then we consider the other possibility when RLS is the first concerted proton-coupled

electron transfer (CPET) step:

$$CO_2 + H_2O + e^- + * \xrightarrow{\overrightarrow{k_{1b}}} COOH^* + OH^- \quad (1b)$$

$$COOH^* + e^- \xrightarrow{\overrightarrow{k_{2b}}} CO^* + OH^- \quad (2b)$$

$$CO^* \underset{\overleftarrow{k_3}}{\overset{\overrightarrow{k_3}}{\rightleftharpoons}} CO + * \quad (3)$$

Note that both reactions (2a) and (2b) are treated as irreversible due to CO oxidation rate can be neglected in the potential window of detectable CO evolution (e.g., more negative than -0.3 V_{RHE} for Au, Cu and glassy carbon supported CoPc). Reaction (3) is quasi-equilibrated because CO adsorption cannot be neglected even on a weak CO-binding metal such as Au [27]. The derivation of these two reaction pathways yields the overall CO_2R rates as:

$$r^a_{CO_2R} = \frac{\overrightarrow{k_{1a}} a_{CO_2}}{1 + K_3 a_{CO}} \quad (4a)$$

$$r^b_{CO_2R} = \frac{\overrightarrow{k_{1b}} a_{CO_2} a_{H_2O}}{1 + K_3 a_{CO}} \quad (4b)$$

in which K_3 is the adsorption equilibrium constant of CO and a_{CO} is the local CO concentration. Considering that $\overrightarrow{k_{1a}} a_{CO_2}$ and $\overrightarrow{k_{1b}} a_{CO_2} a_{H_2O}$ is independent on a_{CO}, the reaction orders of equations (4a) and (4b) with respect to a_{CO} yield the same reaction order expression:

$$\frac{\partial\, ln(r_{CO_2R})}{\partial\, ln(a_{CO})} = \frac{-K_3 a_{CO}}{1 + K_3 a_{CO}} \quad (5)$$

Although equations (4a) and (4b) differ due to the RLS being different, the reaction order expression remains the same. ΔG^{ads}_{CO} is correlated with CO adsorption equilibrium constant:

$$\Delta G^{ads}_{CO} = -k_B T ln(K_3) \quad (6)$$

Combining equations (5) and (6) then the ΔG^{ads}_{CO} can be written as a function of reaction

order ($RO = \frac{\partial\, ln(r_{CO_2R})}{\partial\, l\ (a_{CO})}$) and a_{CO}:

$$\Delta G_{CO}^{ads} = -k_B T ln\left(\frac{-RO}{a_{CO}(RO+1)}\right) \quad (7)$$

Equation (7) is a universal kinetic expression that shows ΔG_{CO}^{ads} on active sites can be determined from RO and a_{CO} regardless of whether RLS is a CO_2 adsorption step or a first CPET step during CO_2R to CO. Equation (7) is visualized in Figure **1** for a better observation of the relationship between ΔG_{CO}^{ads}, CO reaction order and local CO concentration. It is obvious that the active sites with a more negative ΔG_{CO}^{ads} tend to display a more negative CO reaction order at a lower local CO concentration during CO_2R. Thus, to measure ΔG_{CO}^{ads} is equivalent to measure CO reaction order and local CO concentration within the framework of our kinetic model.

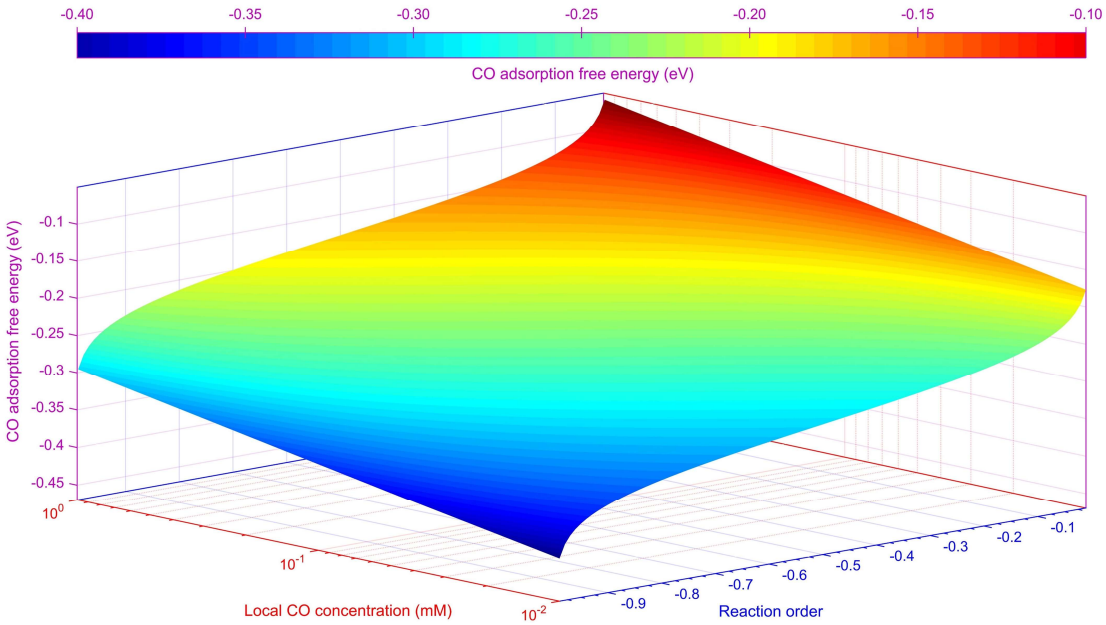

Figure 1. The relationship between the CO adsorption free energy, CO reaction order and local CO concentration derived from equation (7) at 298 K.

Measuring local CO concentrations and reaction orders during CO_2R on polycrystalline Au, Cu and CoPc/GC electrodes

A RRDE voltammetry method was used due to its unique ability to quantify CO reaction orders and local CO concentrations simultaneously during CO_2R to CO [27]. Briefly, an Au ring electrode is a sensitive CO detector that can quantify the CO evolution rate in the presence of co-fed CO during CO_2R, thus CO reaction orders and local CO concentrations can be determined from the Au ring data.

To illustrate the potential of this unique method and show how CO adsorption free energy (ΔG_{CO}^{ads}) varies among different catalysts during CO_2R, the RRDE voltammetry experiments were conducted using Au, Cu and glassy-carbon supported CoPc electrodes. These electrodes were characterized by cyclic voltammetry before and after each measurement as shown in Figures **2a**, **2d** and **2g**, respectively. The corresponding CO partial current densities were shown in Figures **2b**, **2e** and **2h**, thus the CO production activity follows a trend of Au > CoPc/GC > Cu when the activity is compared at the same potential. Note that the lower limit of the potential window was chosen as -0.6 V_{RHE} for Cu due to the adsorbed CO may be further reduced if the applied potential is more negative than -0.6 V_{RHE} in 0.1 M $KHCO_3$ [20,28,29]. Measured reaction orders and local CO concentrations of various catalysts are shown in Figures **2c**, **2f** and **2i**, which suggest Cu electrode displays a more negative ΔG_{CO}^{ads} due to a more negative reaction order was observed at a lower local CO concentration, whereas the ΔG_{CO}^{ads} of Au and CoPc/GC is comparable. A more quantitative comparison of ΔG_{CO}^{ads} among these catalysts is shown in Supplementary Table **1**. These results support that an efficient CO-producing catalyst such as Au or CoPc/GC has a less negative ΔG_{CO}^{ads} to facilitate the CO desorption process to promote the overall CO_2R rate, which can be inferred from equations (4a) and (4b).

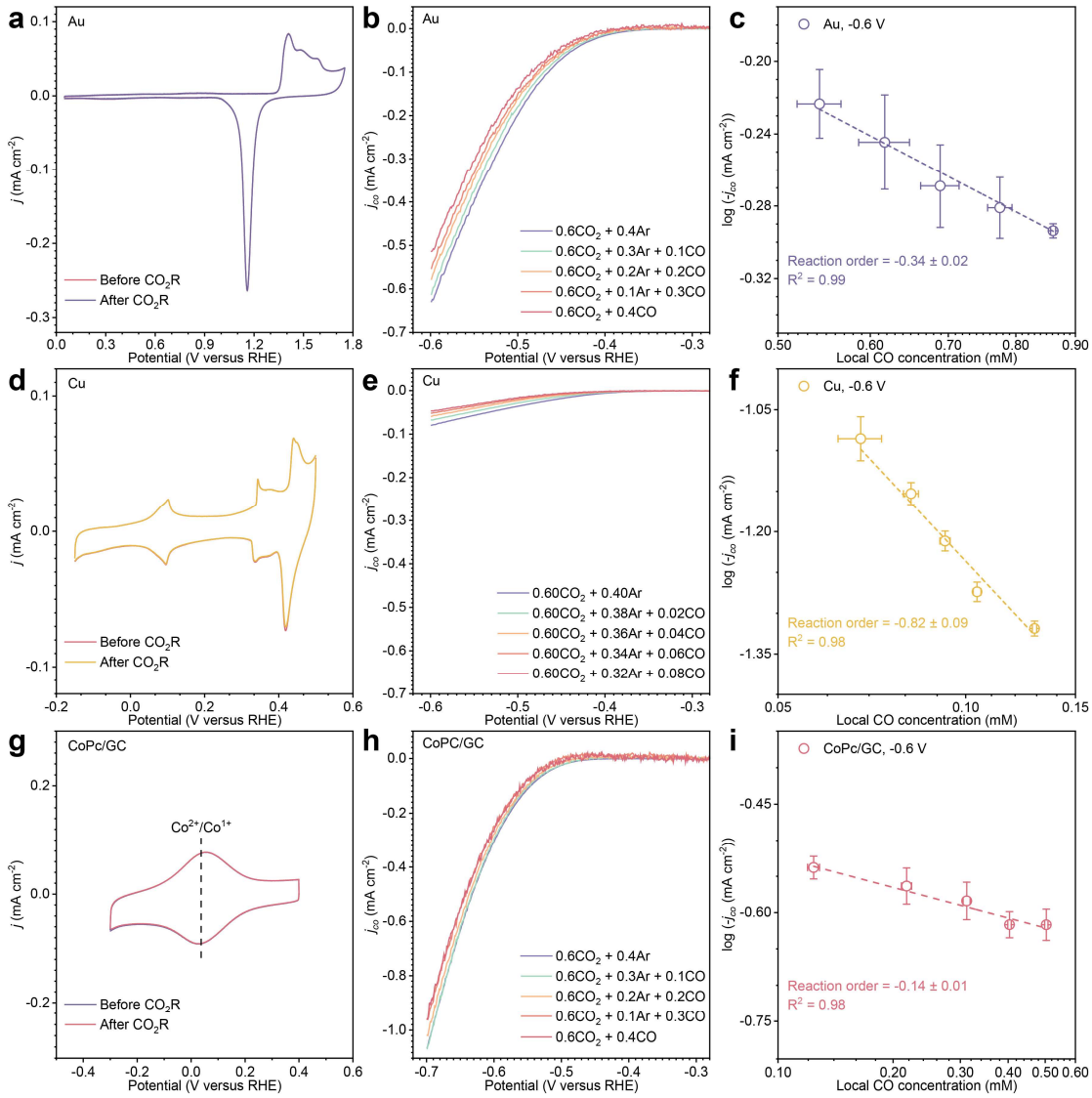

Figure 2. Cyclic voltammetry characterization of **(a)** Au in 0.1 M H_2SO_4 **(d)** Cu in 0.1 M KOH and **(g)** CoPc/GC in 0.1 M $KHCO_3$ recorded at 50 mV s^{-1}, all electrolytes were saturated with Argon. CO partial current densities of **(b)** Au, **(e)** Cu and **(h)** CoPc/GC obtained in 0.1 M $KHCO_3$ from RRDE voltammetry data with a scan rate of 15 mV s^{-1} at 1600 rpm. Measured local CO concentrations and CO reaction orders on **(c)** Au, **(f)** Cu and **(i)** CoPc/GC in 0.1 M $KHCO_3$. Error bars (standard deviations) were estimated from at least three independent measurements.

Electrolyte effects on local CO concentrations and reaction orders measured on a polycrystalline Au electrode

To explore how cation identity impacts the CO adsorption during CO_2R, the local CO concentrations and reaction orders were measured in 0.1 M $LiHCO_3$, $NaHCO_3$ and $KHCO_3$, the corresponding CO partial current densities were shown in Supplementary Figures **5a**, **5b** and Figure **2b**, respectively. Notably, the reaction order is less negative when local CO concentration is higher in 0.1 M $KHCO_3$ as displayed in Figure **3a**, supporting a weaker CO adsorption with less negative ΔG_{CO}^{ads} on Au in $KHCO_3$ electrolyte. The obtained reaction orders and local CO concentrations are comparable in $LiHCO_3$ and $NaHCO_3$, suggesting a similar ΔG_{CO}^{ads} on Au in 0.1 M $LiHCO_3$ and $NaHCO_3$ during CO_2R.

Then local CO concentrations and reaction orders were measured in 0.1 M $NaHCO_3$ + 0.2 M $NaClO_4$ and 0.1 M $NaHCO_3$ + 0.4 M $NaClO_4$ electrolytes to study whether ΔG_{CO}^{ads} shows a dependence on cation concentration. The corresponding CO partial current densities were shown in Supplementary Figures **5c** and **5d**. Figure **3b** illustrates that reaction orders change from -0.50 to -0.94 as the bulk Na^+ concentration increases from 0.1 M to 0.5 M, though local CO concentrations do not display a significant variation. These results reveal that CO adsorption can be enhanced on Au with increasing the cation concentration, however, we considered these results as qualitative evidence due to the local cation concentration is challenging to quantify during CO_2R [30].

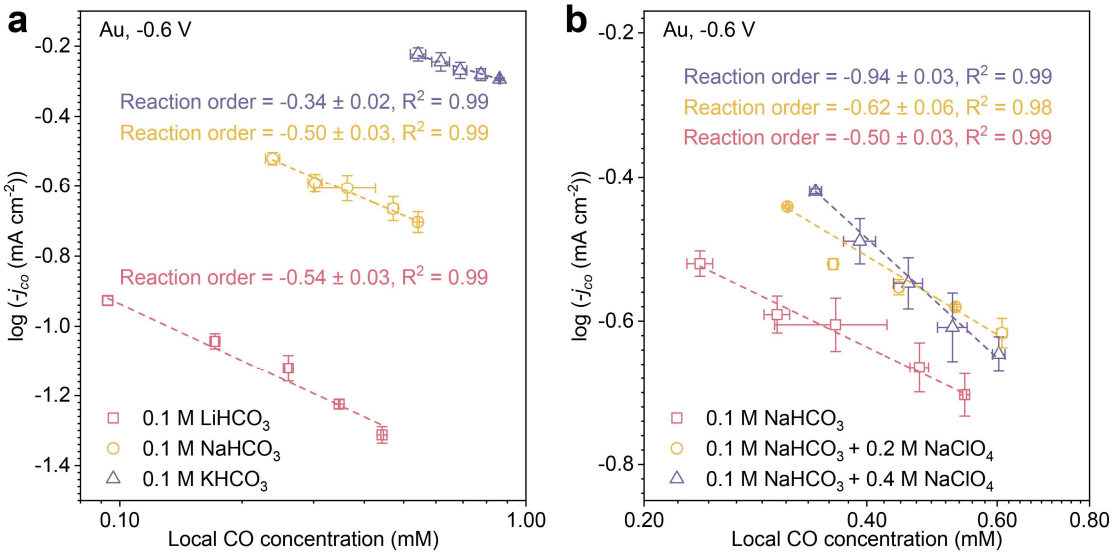

Figure 3. **(a)** Cation identity and **(b)** bulk cation concentration dependence on measured local CO concentrations and CO reaction orders. Error bars (standard deviations) were estimated from at least three independent measurements.

Surface structure effects on local CO concentrations and reaction orders measured on Au(hkl) single crystal electrodes

To demonstrate how surface structure affects the CO adsorption during CO_2R, first the CO partial current densities were measured on Au(110) and Au(111) as shown in Supplementary Figures **6c** and **6d**, respectively. These two electrodes were characterized by cyclic voltammetry as shown in Supplementary Figures **6a** and **6b**, indicating the absence of significant surface roughening induced by the electrochemical lifting during CO_2R measurements [31]. The CO reaction orders and local CO concentrations are shown in Figure **4**, notably, Au(111) displays a near-zero CO reaction order, but Au(110) displays a reaction order of -0.48, which suggests that CO adsorption is more favorable on under-coordinated sites during CO_2R, such as those present on Au(110) surface, and less favorable on close-packed terrace sites, such as those present on the basal plane of Au(111). Furthermore, the obtained reaction orders are almost the same on Au(110) and polycrystalline Au (pcAu). This result further supports that the

active sites are most likely under-coordinated sites on pcAu surface since the active sites of pcAu show a similar reaction order and local CO concentration, thus a similar ΔG_{CO}^{ads} compared to the active surface sites of Au(110), which is consistent with previous studies on determining the active sites for CO_2R on Au [32,33].

These results not only demonstrate the structure-dependence of CO adsorption during CO_2R, but also highlight another potential application of our kinetic model: the active sites for CO_2R on a more complex surface such as polycrystalline surface can be deciphered by comparing the obtained kinetic data (i.e., reaction order of CO) with the data measured from a well-defined single-crystal surface.

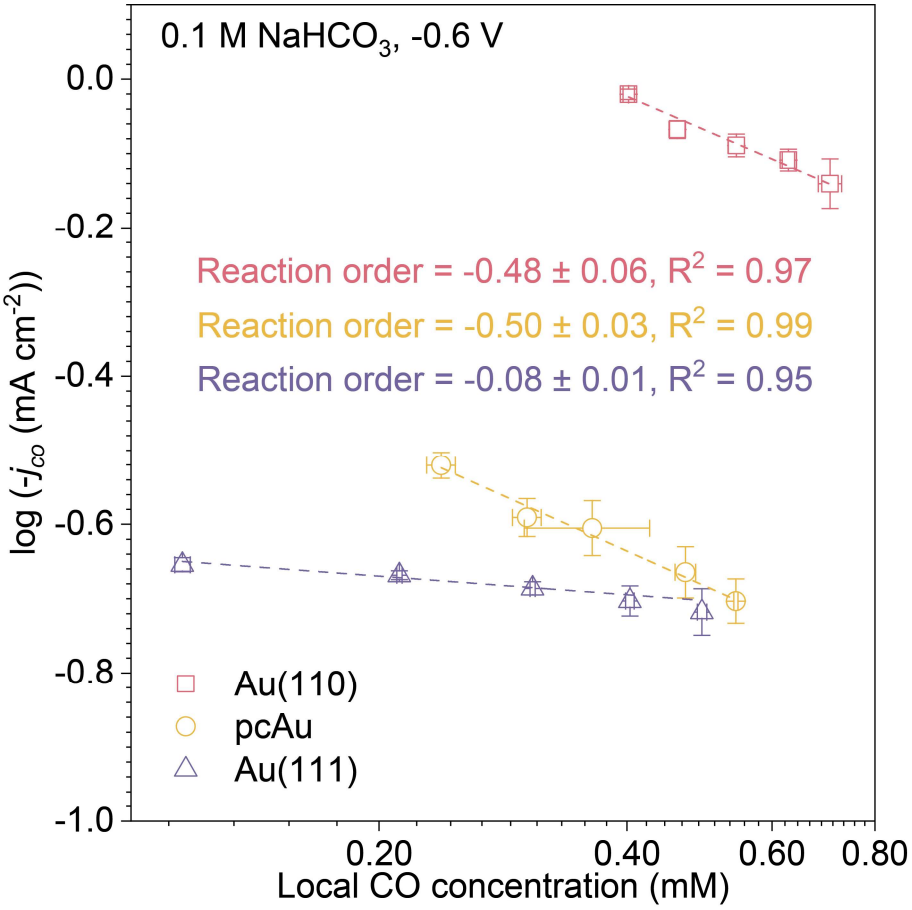

Figure 4. Surface structure dependence on measured local CO concentrations and CO reaction orders. Error bars (standard deviations) were estimated from at least three independent measurements.

A summary of measured CO adsorption free energies and its implications for CO_2R

In this section, we plug all the measured CO reaction orders and local CO concentrations into equation (7) to estimate the CO adsorption free energies under different conditions as shown in Figure **5**. It is obvious that CO adsorption located in an electrode/electrolyte interface under CO_2R condition is much more complex than CO adsorption in a metal/vacuum interface. Specifically, not only the catalyst and surface structure affect CO adsorption, but also applied potential (discussed in more details in our previous work [27]), cation identity and cation concentration play important roles in CO adsorption under CO_2R condition.

The first notable result is that ΔG_{CO}^{ads} obtained in 0.1 M $KHCO_3$ is less negative than ΔG_{CO}^{ads} measured in 0.1 M $LiHCO_3$ and $NaHCO_3$, which suggests a weaker CO adsorption on Au in K^+ containing electrolyte compared to Li^+ and Na^+ electrolytes at CO_2R condition. Furthermore, we observed that CO adsorption could be enhanced (ca. 0.07 eV) at -0.6 V_{RHE} by increasing the bulk Na^+ concentration from 0.1 M to 0.5 M during CO_2R on Au. These results are in agreement with recent spectroscopic studies that Li^+ can enhance CO [34] and CO_2 adsorption on Cu more effectively than other heavier cations such as K^+ and Cs^+, and CO_2 adsorption can be promoted by increasing the cation concentration [35]. Our experimental evidence reveals that the role of cations must be treated explicitly during CO_2R because cations can directly influence the energetics of even a neutral adsorbed intermediate such as CO.

Then ΔG_{CO}^{ads} were compared across different catalysts. Measured ΔG_{CO}^{ads} follows a trend of Cu < Au ≈ CoPc/GC in 0.1 M $KHCO_3$ at -0.6 V_{RHE}, consistent with previous computational predictions that Cu displays a stronger CO adsorption than Au in vacuum [10,36]. However, we argue that our measured ΔG_{CO}^{ads} value difference is quite small (ca. 0.11 eV) between Cu and Au, and ΔG_{CO}^{ads} of $Au_{-0.6\,V}^{0.5\,M\,Na^+}$ is comparable to that of $Cu_{-0.6\,V}^{0.1\,M\,K^+}$. Given that multicarbon products cannot be detected during CO_2R on polycrystalline Au in a broad potential window at ambient conditions [37,38], these results suggest that ΔG_{CO}^{ads} alone is not an efficient descriptor for the formation of multicarbon products during CO_2R, thus the unique CO_2R property of Cu cannot be explained in

terms of ΔG_{CO}^{ads} alone. Other factors such as the interfacial water reactivity [39] and a dual-site model [40,41] should be considered in the reduction of CO_2 to multicarbon products.

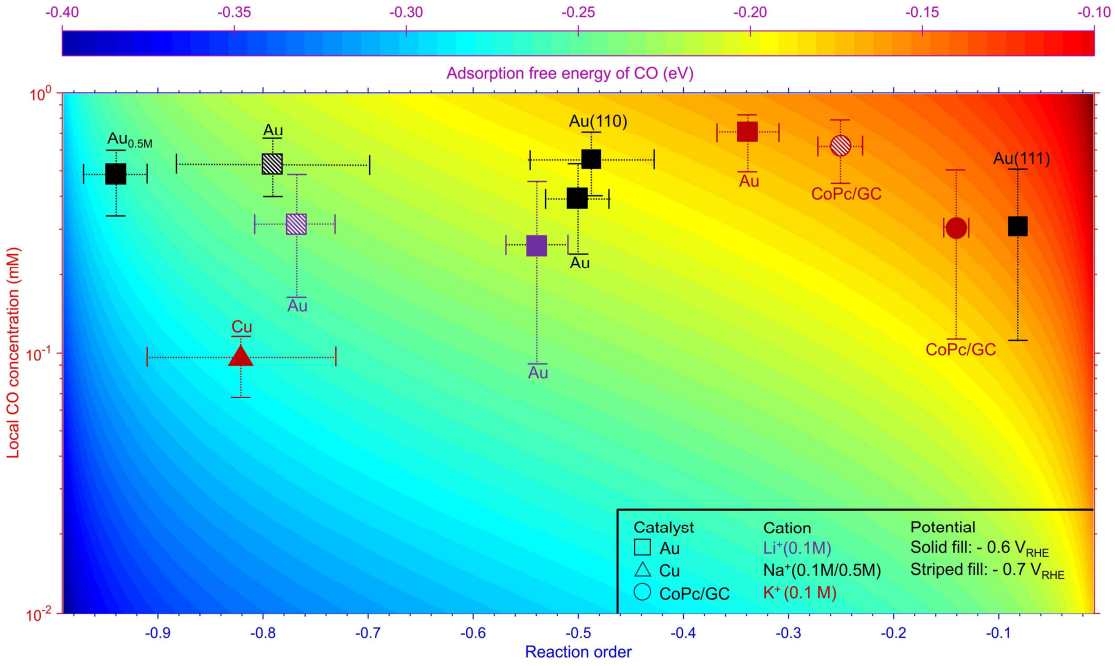

Figure 5. A summary of measured CO adsorption free energies on surface active sites during CO_2R. The bulk cation concentration is 0.1 M unless otherwise specified. Note that the average local CO concentrations were used and error bars were estimated from at least three independent measurements.

Conclusion

In this work, we develop a universal kinetic model for estimating CO adsorption free energy (ΔG_{CO}^{ads}) from measuring local CO concentration and CO reaction order on the CO-producing catalysts. Then we take advantage of a unique RRDE voltammetry method that can measure local CO concentrations and CO reaction orders simultaneously during CO_2R. Measurements of ΔG_{CO}^{ads} unveil that CO adsorption is quite complex at CO_2R condition, which can be influenced by catalyst identity, cation identity, cation concentration, applied potential and surface structure. More importantly, ΔG_{CO}^{ads} alone cannot explain why only Cu catalyzes CO_2 into multicarbon products with substantial rates due to ΔG_{CO}^{ads} difference is insignificant between Au and Cu at CO_2R condition. These results not only highlight the complexity of evaluating energetics of adsorbed intermediate such as CO at CO_2R condition but also provide a universal kinetic method for measuring ΔG_{CO}^{ads} on other CO-producing catalysts during CO_2R.

Methods

Chemicals. The electrolyte solutions were prepared from H_2SO_4(99.999% purity, Sigma-Aldrich), Li_2CO_3(99.999%, Thermo Scientific Chemicals), Na_2CO_3(99.999%, Thermo Scientific Chemicals), K_2CO_3(99.997%, Thermo Scientific Chemicals), KOH(99.98%, Thermo Scientific Chemicals), $NaClO_4$(99.9%, Sigma Aldrich), Chelex-100(sodium form, 50-100 mesh, Sigma-Aldrich), and ultrapure water (Millipore Milli-Q®, IQ7000, ≥ 18.2 MΩ·cm, TOC < 2.5 ppb). Ar(99.998%, Linde), CO(99.99%, Linde), CO_2(99.999%, Linde), H_2(99.995%, Linde) were used for purging the electrolyte solutions.

Polycrystalline Au disk and ring electrodes preparation. Prior to each experiment, the gold disk (99.99%, diameter: 5 mm, thickness: 4 mm, Pine Instruments) and ring electrodes (geometric surface area ≈ 0.110 cm^2, 99.99%, Pine Instruments) were mechanically polished on Buehler polishing cloth with decreasing sizes of 1, 0.25 and 0.1 μm diamond suspensions (Electron Microscopy Sciences). Next, the RRDE tip was sonicated in acetone and ultrapure water three times to remove any impurities attached to the RRDE tip. Then the RRDE tip was transferred to the electrochemical polishing cell, gold disk electrode and gold ring electrode were short-circuited and cycled between 0.05 and 1.75 V_{RHE} for 100 cycles at 1 V s^{-1} in Ar saturated 0.1 M H_2SO_4.

CoPc/GC disk electrode and Au ring electrode preparation. Catalyst ink was prepared by dispersing 10 mg of cobalt phthalocyanine (Sigma Aldrich) in a mixture of 100 μL of 5 wt.% Nafion solution (Nafion 117, 5 wt.%) and 3900 μL N,N-dimethylformamide (DMF, Sigma Aldrich, 99.9%) with 1 hour of sonication to yield a final solution containing a CoPc concentration of ca. 4.38×10^{-3} M. Prior to each experiment, the glassy carbon disk electrode (99.99%, diameter: 5 mm, thickness: 4 mm, Pine Instruments) and Au ring electrode were separately polished on Buehler

polishing cloth with decreasing sizes of 1, 0.25 and 0.1 μm diamond suspensions. Next, the RRDE tip was assembled and sonicated in acetone and ultrapure water three times to remove any impurities attached to the RRDE tip. The RRDE tip was transferred to the electrochemical polishing cell, Au ring electrode was cycled between 0.05 and 1.75 V_{RHE} for 100 cycles at 1 V s^{-1} in Ar saturated 0.1 M H_2SO_4. Then CoPc/GC disk electrode was prepared by dropcasting 10 μL of the prepared ink onto the center of glassy carbon (loading: ca. 0.13 mg cm^{-2}). The droplet spreads throughout the entire glassy carbon disk without contacting the Au ring electrode. The electrode was then oven-dried at 60 °C for 15 min.

Polycrystalline Cu disk electrode and Au ring electrode preparation. Prior to each experiment, the Cu disk electrode (99.99%, diameter: 5 mm, thickness: 4 mm, Pine Instruments) and Au ring electrode were separately polished on Buehler polishing cloth with decreasing sizes of 1, 0.25 and 0.1 μm diamond suspensions. Then the electrodes were transferred to two electrochemical polishing cells, Au ring electrode was cycled between 0.05 and 1.75 V_{RHE} for 100 cycles at 1 V s^{-1} in Ar saturated 0.1 M H_2SO_4 and Cu disk electrode was polarized to 1.3 V_{RHE} for 3 mins in 66% H_3PO_4. The electrodes were rinsed through ultrapure water after the electrochemical polishing process. Next, the RRDE tip was assembled and rinsed in ultrapure water.

Single crystal Au disk electrode and Au ring electrode preparation. Prior to each experiment, the single crystal Au disk electrodes (99.999%, diameter: 5 mm, thickness: 4 mm, Princeton Scientific) were flame-annealed to red heat for ca. 10 s using a propane torch and cooled down in an Argon stream. The Au ring electrode was polished on Buehler polishing cloth with decreasing sizes of 1, 0.25 and 0.1 μm diamond suspensions, then the ring electrode was sonicated in acetone and ultrapure water three times. Next the RRDE tip was assembled and transferred to the electrochemical

polishing cell under the potential control, Au single crystal disk electrode was held at 0.1 V_{RHE} while the Au ring electrode was cycled between 0.05 and 1.75 V_{RHE} for 100 cycles at 1 V s^{-1} and 400 rpm in Ar saturated 0.1 M H_2SO_4.

Purification of electrolyte. To prepare electrolyte solutions with ultralow content of polyvalent metallic impurities, M_2CO_3(M = Li, Na and K, trace metal basis) and disposable polystyrene spoons (VWR) were used to prepare 0.05 M_2CO_3 solution with ultrapure water in a clean polystyrene plastic bottle to avoid any possible trace metal contamination from the glassware, then approximately 30 g Chelex-100 per mole of M_2CO_3 was added to the solution and then this mixture was stirred at 700 rpm for 24 h. Next, insoluble Chelex-100 resin particles were removed from the electrolyte solution by vacuum filtration with the help of a PES membrane (Polyethersulfone, pore size: 0.45µm, VWR). The filtered solution volume was adjusted using a 1 L PMP plastic volumetric flask (BRAND®), and the ultrapure electrolyte solution was stored in a clean polystyrene bottle.

Prior to each independent experiment, 100 mL of 0.05 M carbonate solution was bubbled through CO_2 for 1 hour with a flow rate of 120 sccm (Standard cubic centimeters per minute) using a mass flow controller (Sierra Instruments) to convert 0.05 M carbonate solution to 0.1 M bicarbonate solution. The electrolyte purity was further checked using electrochemical characterizations described in a previous work [42].

General electrochemical measurements. All the electrochemical measurements were carried out in homemade standard three-electrode glass cells. The counter electrode was a high-purity graphite rod (99.9995%, Thermo Scientific Chemicals) separated from the working compartment with a porous glass frit. Either a homemade reversible hydrogen electrode (RHE) or a leak-free Ag/AgCl reference electrode (3.4 M KCl,

Innovative Instruments) was used as the reference electrode, which was separated from the working compartment through a homemade Luggin capillary. All the glassware was rinsed and sonicated before each independent experiment with diluted Piranha solution and boiling ultrapure water three times. For all measurements, 85% ohmic drop compensation was performed using a CHI 760D bipotentiostat (CH Instruments), and the remaining 15% drop was compensated manually after the experiment. The ohmic drop of the system was determined by carrying out potentiostatic electrochemical impedance spectroscopy (PEIS) at 0.10 V_{RHE} (ΔV = 10 mV, from 100 kHz to 1 Hz). The Ohmic resistance of the cell (R_u) was obtained by extrapolation of the fitted modified Randles equivalent circuit with a constant phase element. The measured potentials were converted to RHE scale by $E_{RHE} = E_{Ag/AgCl} + 0.210\ V + 0.059\ V \times pH$.

RRDE experiments. To perform CO_2R study using a RRDE setup, the disk and ring electrodes were prepared as mentioned before. The measurements were conducted in CO_2/CO/Ar saturated 0.1 M $MHCO_3$ electrolyte solution (M= Li, Na or K, pH ≈ 7, T = 25 ± 1 °C). First the ring electrode potential was set to 1.05 V_{RHE} and the disk electrode was held at open circuit potential (ca. 0.5 V_{RHE} in CO_2/Ar saturated electrolytes) to collect the ring current background, then the disk was scanned to more negative potentials at 15 mV s^{-1} to conduct CO_2R while the ring potential was set to 1.05 V_{RHE} once a stable ring background current was recorded. The collection efficiency was measured immediately following the RRDE experiment and voltametric surface characterization. The RRDE tip suffered from bubble attachment issue due to higher total current densities obtained at extremely negative potentials, thus the most negative potential was chosen to be -0.70 V_{RHE}. The flow of CO_2/CO/Ar gas mixture was controlled by three mass flow controllers (Sierra Instruments and Alicat Scientific). Before RRDE measurements, the flow rate of each mass flow controller was checked

using a mass flow meter (Sierra Instruments).

The electrochemical surface area (ECSA) determination. Following CO_2R experiment, a characterization cyclic voltammetry (CV) of the Au disk electrode was obtained between 0.05 and 1.75 V_{RHE} at a scan rate of 50 mV s^{-1}. The electrochemically active surface area (ECSA) of the polycrystalline Au electrode was determined by calculating the total charge from integrating the reduction peak in the characterization CV and dividing it by the specific charge corresponds to the reduction of one monolayer of gold monoxide (386 μC cm^{-2}) [43]. The CV of the lead under-potential deposition (Pb-UPD) on Cu was performed at a pH of ca. 3 using an electrolyte solution of 0.1 M $NaClO_4$ + 1 mM NaCl + 2 mM $Pb(ClO_4)_2$ + 1 mM $HClO_4$. The cyclic voltammograms were recorded between −0.4 V and −0.2 V versus Ag/AgCl with a scan rate of 5 mV s^{-1}, a representative result is shown in Supplementary Figure **1**. The ECSA of Cu was determined using the integrated charge under the cathodic curves of the Pb-UPD CV and dividing it by the specific charge corresponds to a smooth polycrystalline Cu surface (357 μC cm^{-2}) [44]. The geometric surface area (0.196 cm^2) was used as ECSA for Au single crystal and CoPc/GC electrodes.

Collection efficiency determination. Following each RRDE experiment, the apparent collection efficiency (N) was determined in a separate cell containing Ar saturated 0.1 M sodium phosphates buffer (pH=6.9) with 5 mM $K_3Fe(CN)_6$. The disk was cycled between 0.10 and 0.30 V_{RHE} and the ring potential was set to 1.10 V_{RHE}, a representative result is shown in Supplementary Figure **2**. The apparent collection efficiency was calculated according to equation (8).

$$N = \left|\frac{i_{ring}}{i_{disk}}\right| \tag{8}$$

RRDE data processing. The partial current density of CO evolution is calculated from

the background subtracted ring current ($i_{ring} - i_{background}$), the apparent collection efficiency (N) and the electrochemically active surface area of the disk ($ECSA_{disk}$) as

$$j_{co} = \frac{-(i_{ring} - i_{background})}{N \times ECSA_{disk}} \quad (9)$$

The local CO concentration (a_{CO}) near the disk electrode can be calculated as

$$a_{CO} = a_{CO}^{feed} + a_{CO}^{CO_2R} \quad (10)$$

where a_{CO}^{feed} and $a_{CO}^{CO_2R}$ are the concentrations of co-fed CO and CO generated from the CO_2R, respectively. The $a_{CO}^{CO_2R}$ is estimated by using a well-defined concentration profile of RRDE [45,46] as below:

$$a_{CO}^{CO_2R} = \frac{0.1 \times h \times \left(i_{ring} - i_{background}\right)}{i_{ring}^{0.1atm\ CO} \times N} \quad (11)$$

in which $i_{ring}^{0.1atm\ CO}$ is the mass-transport limited CO oxidation current collected on the Au ring electrode in $0.6CO_2/0.3Ar/0.1CO$ saturated 0.1 M bicarbonate electrolyte solution, h is Henry's law constant of CO (ca. 10^{-3} mol l^{-1} atm^{-1}) at 298 K in aqueous media [47]. Note that this method averages CO concentrations in the lateral direction of the disk electrode to estimate the local CO concentration generated from CO_2R.

Acknowledgements

This work was supported by the National Science Foundation (NSF CHE 1455162) and in part by the Ohio State University Department of Chemistry and Biochemistry.

Notes

The authors declare no competing financial interest.

References

1 Hori, Y. in *Modern Aspects of Electrochemistry* (eds Constantinos G. Vayenas, Ralph E. White, & Maria E. Gamboa-Aldeco) 89-189 (Springer New York, 2008).

2 Zhang, S., Fan, Q., Xia, R. & Meyer, T. J. CO2 Reduction: From Homogeneous to Heterogeneous Electrocatalysis. *Accounts of Chemical Research* **53**, 255-264, doi:10.1021/acs.accounts.9b00496 (2020).

3 Nitopi, S. *et al.* Progress and Perspectives of Electrochemical CO2 Reduction on Copper in Aqueous Electrolyte. *Chemical Reviews* **119**, 7610-7672, doi:10.1021/acs.chemrev.8b00705 (2019).

4 Zhou, Y. *et al.* Long-chain hydrocarbons by CO2 electroreduction using polarized nickel catalysts. *Nature Catalysis* **5**, 545-554, doi:10.1038/s41929-022-00803-5 (2022).

5 Clark, E. L., Hahn, C., Jaramillo, T. F. & Bell, A. T. Electrochemical CO2 Reduction over Compressively Strained CuAg Surface Alloys with Enhanced Multi-Carbon Oxygenate Selectivity. *Journal of the American Chemical Society* **139**, 15848-15857, doi:10.1021/jacs.7b08607 (2017).

6 Morales-Guio, C. G. *et al.* Improved CO2 reduction activity towards C2+ alcohols on a tandem gold on copper electrocatalyst. *Nature Catalysis* **1**, 764-771, doi:10.1038/s41929-018-0139-9 (2018).

7 Kim, D., Resasco, J., Yu, Y., Asiri, A. M. & Yang, P. Synergistic geometric and electronic effects for electrochemical reduction of carbon dioxide using gold–copper bimetallic nanoparticles. *Nature Communications* **5**, 4948, doi:10.1038/ncomms5948 (2014).

8 Ren, D., Ang, B. S.-H. & Yeo, B. S. Tuning the Selectivity of Carbon Dioxide Electroreduction toward Ethanol on Oxide-Derived CuxZn Catalysts. *ACS Catalysis* **6**, 8239-8247, doi:10.1021/acscatal.6b02162 (2016).

9 Vos, R. E. & Koper, M. T. M. Nickel as Electrocatalyst for CO(2) Reduction: Effect of Temperature, Potential, Partial Pressure, and Electrolyte Composition. *ACS Catalysis* **14**, 4432-4440, doi:10.1021/acscatal.4c00009 (2024).

10 Bagger, A., Ju, W., Varela, A. S., Strasser, P. & Rossmeisl, J. Electrochemical CO2 Reduction: A Classification Problem. *ChemPhysChem* **18**, 3266-3273, doi:https://doi.org/10.1002/cphc.201700736 (2017).

11 Wong, A. J.-W. Sensitivity Analysis of Electrochemical Double Layer Approximations on Electrokinetic Predictions: Case Study for CO Reduction on Copper. *Journal of physical chemistry. C* **128**, 10837-10847, doi:10.1021/acs.jpcc.4c01457.

12 Lucky, C. & Schreier, M. Mind the Interface: The Role of Adsorption in Electrocatalysis. *ACS Nano* **18**, 6008-6015, doi:10.1021/acsnano.3c09523 (2024).
13 Cui, Z. *et al.* Unraveling the electrocatalytic reduction mechanism of enols on copper in aqueous media. *Nature Communications* **13**, 5840, doi:10.1038/s41467-022-33620-2 (2022).
14 Tran, B. & Goldsmith, B. R. Theoretical Investigation of the Potential-Dependent CO Adsorption on Copper Electrodes. *The Journal of Physical Chemistry Letters* **15**, 6538-6543, doi:10.1021/acs.jpclett.4c01032 (2024).
15 Ryberg, R. Carbon monoxide adsorbed on Cu(100) Studied by infrared spectroscopy. *Surface Science* **114**, 627-641, doi:https://doi.org/10.1016/0039-6028(82)90710-5 (1982).
16 Gottfried, J. M., Schmidt, K. J., Schroeder, S. L. M. & Christmann, K. Adsorption of carbon monoxide on Au(110)-(1×2). *Surface Science* **536**, 206-224, doi:https://doi.org/10.1016/S0039-6028(03)00595-8 (2003).
17 Le Rouzo, H., Parneix, P., Raşeev, G. & Smirnov, K. S. Adsorption sites and migration of a carbon monoxide molecule on stepped vicinal surfaces of Cu(211) and Cu(511). *Surface Science* **415**, 131-147, doi:https://doi.org/10.1016/S0039-6028(98)00527-5 (1998).
18 Xiong, H. *et al.* Correlating the Experimentally Determined CO Adsorption Enthalpy with the Electrochemical CO Reduction Performance on Cu Surfaces. *Angewandte Chemie International Edition* **62**, e202218447, doi:https://doi.org/10.1002/anie.202218447 (2023).
19 Gao, W. *et al.* CO Binding Energy is an Incomplete Descriptor of Cu-Based Catalysts for the Electrochemical CO2 Reduction Reaction. *Angewandte Chemie International Edition* **62**, e202313798, doi:https://doi.org/10.1002/anie.202313798 (2023).
20 Li, C. W. & Kanan, M. W. CO2 Reduction at Low Overpotential on Cu Electrodes Resulting from the Reduction of Thick Cu2O Films. *Journal of the American Chemical Society* **134**, 7231-7234, doi:10.1021/ja3010978 (2012).
21 Zeng, J. S., Corbin, N., Williams, K. & Manthiram, K. Kinetic Analysis on the Role of Bicarbonate in Carbon Dioxide Electroreduction at Immobilized Cobalt Phthalocyanine. *ACS Catalysis* **10**, 4326-4336, doi:10.1021/acscatal.9b05272 (2020).
22 Deng, W., Zhang, P., Seger, B. & Gong, J. Unraveling the rate-limiting step of two-electron transfer electrochemical reduction of carbon dioxide. *Nature Communications* **13**, 803, doi:10.1038/s41467-022-28436-z (2022).
23 Hsu, Y.-S., Rathnayake, S. T. & Waegele, M. M. Cation effects in hydrogen evolution and CO2-to-CO conversion: A critical perspective. *The Journal of Chemical Physics* **160**, doi:10.1063/5.0201751 (2024).
24 Zhu, X., Huang, J. & Eikerling, M. Electrochemical CO2 Reduction at Silver from a Local Perspective. *ACS Catalysis* **11**, 14521-14532, doi:10.1021/acscatal.1c04791 (2021).
25 Clark, E. L. *et al.* Influence of Atomic Surface Structure on the Activity of Ag for the Electrochemical Reduction of CO2 to CO. *ACS Catalysis* **9**, 4006-4014, doi:10.1021/acscatal.9b00260 (2019).
26 Vijay, S. *et al.* Unified mechanistic understanding of CO2 reduction to CO on transition metal and single atom catalysts. *Nature Catalysis* **4**, 1024-1031, doi:10.1038/s41929-021-00705-y (2021).
27 Cui, Z., Wong, A. J.-W., Janik, M. J. & Co, A. C. Negative Reaction Order for

CO during CO2 Electroreduction on Au. *Journal of the American Chemical Society*, doi:10.1021/jacs.4c06232 (2024).
28 Huang, Y., Handoko, A. D., Hirunsit, P. & Yeo, B. S. Electrochemical Reduction of CO2 Using Copper Single-Crystal Surfaces: Effects of CO* Coverage on the Selective Formation of Ethylene. *ACS Catalysis* **7**, 1749-1756, doi:10.1021/acscatal.6b03147 (2017).
29 Heyes, J., Dunwell, M. & Xu, B. CO2 Reduction on Cu at Low Overpotentials with Surface-Enhanced in Situ Spectroscopy. *The Journal of Physical Chemistry C* **120**, 17334-17341, doi:10.1021/acs.jpcc.6b03065 (2016).
30 Koper, M. T. M. Theory and kinetic modeling of electrochemical cation-coupled electron transfer reactions. *Journal of Solid State Electrochemistry* **28**, 1601-1606, doi:10.1007/s10008-023-05653-0 (2024).
31 Dakkouri, A. & Kolb, D. *Reconstruction of gold surfaces*. (Marcel Dekker: New York, 1999).
32 Todoroki, N. *et al.* Surface Atomic Arrangement Dependence of Electrochemical CO2 Reduction on Gold: Online Electrochemical Mass Spectrometric Study on Low-Index Au(hkl) Surfaces. *ACS Catalysis* **9**, 1383-1388, doi:10.1021/acscatal.8b04852 (2019).
33 Mezzavilla, S., Horch, S., Stephens, I. E. L., Seger, B. & Chorkendorff, I. Structure Sensitivity in the Electrocatalytic Reduction of CO2 with Gold Catalysts. *Angewandte Chemie International Edition* **58**, 3774-3778, doi:https://doi.org/10.1002/anie.201811422 (2019).
34 Xu, Y., Xia, Z., Gao, W., Xiao, H. & Xu, B. Cation effect on the elementary steps of the electrochemical CO reduction reaction on Cu. *Nature Catalysis*, doi:10.1038/s41929-024-01227-z (2024).
35 Zhang, Z.-M. *et al.* Probing electrolyte effects on cation-enhanced CO2 reduction on copper in acidic media. *Nature Catalysis*, doi:10.1038/s41929-024-01179-4 (2024).
36 Patra, A., Peng, H., Sun, J. & Perdew, J. P. Rethinking CO adsorption on transition-metal surfaces: Effect of density-driven self-interaction errors. *Physical Review B* **100**, 035442, doi:10.1103/PhysRevB.100.035442 (2019).
37 Chen, Y., Li, C. W. & Kanan, M. W. Aqueous CO2 Reduction at Very Low Overpotential on Oxide-Derived Au Nanoparticles. *Journal of the American Chemical Society* **134**, 19969-19972, doi:10.1021/ja309317u (2012).
38 Marcandalli, G., Monteiro, M. C. O., Goyal, A. & Koper, M. T. M. Electrolyte Effects on CO2 Electrochemical Reduction to CO. *Accounts of Chemical Research* **55**, 1900-1911, doi:10.1021/acs.accounts.2c00080 (2022).
39 Winkler, D., Leitner, M., Auer, A. & Kunze-Liebhäuser, J. The Relevance of the Interfacial Water Reactivity for Electrochemical CO Reduction on Copper Single Crystals. *ACS Catalysis* **14**, 1098-1106, doi:10.1021/acscatal.3c02700 (2024).
40 Gao, W., Xu, Y., Fu, L., Chang, X. & Xu, B. Experimental evidence of distinct sites for CO2-to-CO and CO conversion on Cu in the electrochemical CO2 reduction reaction. *Nature Catalysis* **6**, 885-894, doi:10.1038/s41929-023-01002-6 (2023).
41 Verdaguer-Casadevall, A. *et al.* Probing the Active Surface Sites for CO Reduction on Oxide-Derived Copper Electrocatalysts. *Journal of the American Chemical Society* **137**, 9808-9811, doi:10.1021/jacs.5b06227 (2015).
42 Cui, Z., Marx, M. A., Tegomoh, M. N. & Co, A. C. A Guide to Evaluate Electrolyte Purity for CO2 Reduction Studies. *ACS Energy Letters*, 5201-5205,

doi:10.1021/acsenergylett.3c02343 (2023).
43 Rand, D. A. J. & Woods, R. The nature of adsorbed oxygen on rhodium, palladium and gold electrodes. *Journal of Electroanalytical Chemistry and Interfacial Electrochemistry* **31**, 29-38, doi:https://doi.org/10.1016/S0022-0728(71)80039-6 (1971).
44 Sebastián-Pascual, P. & Escudero-Escribano, M. Surface characterization of copper electrocatalysts by lead underpotential deposition. *Journal of Electroanalytical Chemistry* **896**, 115446, doi:https://doi.org/10.1016/j.jelechem.2021.115446 (2021).
45 Albery, W. J. Ring-disc electrodes. Part 1.—A new approach to the theory. *Transactions of the Faraday Society* **62**, 1915-1919, doi:10.1039/TF9666201915 (1966).
46 Albery, W. J. & Bruckenstein, S. Ring-disc electrodes. Part 2.—Theoretical and experimental collection effciencies. *Transactions of the Faraday Society* **62**, 1920-1931, doi:10.1039/TF9666201920 (1966).
47 Sander, R. Compilation of Henry's law constants (version 5.0.0) for water as solvent. *Atmos. Chem. Phys.* **23**, 10901-12440, doi:10.5194/acp-23-10901-2023 (2023).